

Near infrared fluorescent optical imaging for nodal staging

Lakshmi Sampath

Baylor College of Medicine
Division of Molecular Imaging
Department of Radiology
and
Molecular Physiology and Biophysics
and
The Baylor Breast Center
Houston, Texas 77030

Wei Wang

Baylor College of Medicine
Division of Molecular Imaging
Department of Radiology
Houston, Texas 77030

Eva M. Sevick-Muraca

Baylor College of Medicine
Division of Molecular Imaging
Department of Radiology
and
Molecular Physiology and Biophysics
and
The Baylor Breast Center
Houston, Texas 77030

Abstract. Current techniques to assess lymph node metastases in cancer patients include lymphoscintigraphy after administration of a non-specific radiocolloid in order to locate and resect lymph nodes for pathological examination of harbored cancer cells. Clinical trials involving intradermal or subcutaneous injection of antibody-based nuclear imaging agents have demonstrated the feasibility for target-specific, molecular imaging of cancer-positive lymph nodes. The basis for employing near-infrared (NIR) optical imaging for assessing disease is evidenced by recent work showing functional lymph imaging in mice, swine, and humans. We review antibody-based immunolymphoscintigraphy with an emphasis on the use of trastuzumab (or Herceptin) to target human epidermal growth factor receptor-2 (HER2) overexpressed in some breast cancers. Specifically, we review *in vitro* and preclinical imaging data from our laboratory that show how the dual-labeled agent $(^{111}\text{In-DTPA})_n\text{-trastuzumab-(IRDye800)}_m$ utilizes the high photon count provided by an NIR fluorescent dye, IRDye 800CW, and the radioactive signal from a gamma emitter, Indium-111, for possible detection of HER2 metastasis in lymph nodes. We show that the accumulation and clearance of $(^{111}\text{In-DTPA})_n\text{-trastuzumab-(IRDye800)}_m$ from the axillary nodes of mice occurs 48 h after intradermal injection into the dorsal aspect of the foot. The requirement for long clearance times from normal, cancer-negative nodes presents challenges for nuclear imaging agents with limited half-lives but does not hamper NIR optical imaging.

© 2008 Society of Photo-Optical Instrumentation Engineers. [DOI: 10.1117/1.2953498]

Keywords: fluorescence imaging; breast cancer; human epidermal growth factor receptor-2, (HER2); lymph node staging; intradermal administration.

Paper 07409SSRR received Sep. 29, 2007; revised manuscript received May 4, 2008; accepted for publication May 8, 2008; published online Jul. 16, 2008.

1 Introduction

Nodal staging plays a critical role in the evaluation of disease progression and design of therapeutic strategies in the treatment of most cancer patients. For example, in breast cancer, intradermal (i.d.) or subcutaneous (s.c.) administration of a nonspecific $^{99\text{m}}\text{Tc}$ -radiocolloid is used to identify the tumor draining or sentinel lymph node for resection. Once the surgical pathologist confirms the presence of cancer cells in the resected sentinel lymph node, additional nodes around the axilla are removed to better assess the extent of lymph node involvement. The accuracy of nodal staging is critical for judicious selection of effective therapy. The inability to surgically resect inaccessible tumor-draining lymph nodes, such as the internal mammary or supraclavicular lymph nodes in breast cancer patients, or the pelvic lymph nodes that drain the prostate in prostate cancer patients, can compromise oncologists' ability to accurately stage and select proper therapy. Noninvasive, diagnostic imaging of cancer-positive lymph

nodes could positively impact the manner in which tumor-node-metastasis (TNM) staging is performed.

Molecular imaging approaches for early-stage diagnosis of metastasis in the lymphatics were first explored by Weinstein et al., who used radio-labeled monoclonal antibodies that were administered (i.d.) through the footpad in preclinical studies.^{1,2} Since then, several investigators have used immunolymphoscintigraphy as a tool to study lymphatic delivery of agents. Steller et al.³ demonstrated the dose dependence of iodinated monoclonal antibody biodistribution following i.d. administration in a murine animal model, while Wahl et al.⁴ employed iodinated intact and fragmented antibodies to assess the kinetics of their clearance from the lymphatic system in response to ambulation. Additional reports have used immunolymphoscintigraphy to study lung cancer metastases to pulmonary and mediastinal lymph nodes in dogs.⁵ The i.d. route of imaging agent delivery may be extremely favorable for nodal staging because antibodies and small molecules drain primarily from the lymph plexus into the lymphatic system. Small molecules pass readily through one or more nodes before exiting the lymphatic circulation via the blood circulatory

Address all correspondence to: Eva M. Sevick-Muraca, Ph.D., One Baylor Plaza, BCM 360, Baylor College of Medicine, Houston, Texas 77030. Tel: 713-798-3684; Fax: 713-798-2749; E-mail: evas@bcm.edu

system, while larger agents may be retained longer within lymph nodes. Some advantages for using a direct lymphatic approach include: (1) high lymph node uptake of antibodies, which enables significantly lower doses of labeled antibodies than that required for intravenous (i.v.) administration, (2) more rapid lymph node uptake, enabling minimal time between i.d. antibody administration and imaging, and (3) increased target-to-background ratios due to reduced nonspecific binding, which would otherwise occur in systemic i.v. administration. A more comprehensive review of lymphatic uptake and transport of proteins following intralymphatic administration can be found in an article by Porter and Charman.⁶

In addition to animal studies, imaging-based clinical applications of intralymphatic administration have also been explored by several investigators, mostly using radio-labeled monoclonal antibodies in their intact or fragmented form to detect tumor-draining lymph nodes in a spectrum of cancer patients ranging from melanoma, T-cell lymphoma, breast, and prostate cancers. One of the first investigations of lymph node imaging was reported by Order et al. in 1975, in which they demonstrated accumulation of ¹³¹I-labeled antiferrin immunoglobulin in lymph nodes of patients with breast carcinoma and lymphoma.⁷

Following that, DeLand et al. conjugated ¹³¹I-labeled antibodies to carcinoembryonic antigen (CEA) and showed high sensitivity in detecting nodal metastases after interdigital administration in patients.⁸ In breast cancer and T-cell lymphoma, immunolymphoscintigraphy was performed by several investigators with ¹³¹I-, ¹¹¹In-, and ^{99m}Tc-labeled monoclonal antibodies to noninvasively assess regional lymph nodes.^{9–12} Pelvic nodal metastases in prostate cancer have been investigated¹³ by bipedal intralymphatic administration of ¹¹¹In-PAY 276, while antimelanoma antibodies that have been radio-labeled for lymphoscintigraphy have also been reported in the literature.^{14–16} Most injections were well tolerated, but some patients have reported pain at the injection site. Most studies have reported a high sensitivity (80 to 100%) using this route of administration, but nonspecific uptake by normal lymph nodes continues to be problematic.

Although lymphoscintigraphy, or the administration of nonspecific ^{99m}Tc sulfur colloid, is the “gold standard” for clinically evaluating lymph mapping, some limitations suffered by this imaging technique include the need for long (~20 min) gamma camera integration times, poor temporal and spatial resolution, low signal-to-noise ratios (SNRs), and the finite physical half-life of the tracer [$t_{1/2}(\text{}^{99\text{m}}\text{Tc})=6\text{ h}$]. In contrast, near-infrared (NIR) fluorophores provide an attractive opportunity that outweighs some of these disadvantages inherent in nuclear techniques. Since fluorescent reporters do not have a physical half-life, they can be repeatedly activated using appropriate excitation light. Theoretically, for a fluorophore with a nanosecond fluorescent lifetime and a quantum efficiency of 0.1, 10^8 photons can be generated per second per molecule. When compared to the one-photon imaging event resulting from the radioactive decay of a radionuclide, the potential advantages of NIR fluorescent optical imaging with NIR fluorophores becomes evident. The increased photon yield can considerably improve signal-to-noise and significantly reduce image acquisition time for molecular imaging,

if tissue attenuation does not significantly reduce the number of detected fluorescent photons. While NIR fluorophores also have an absorption cross section, their administration in trace doses does not provide sufficient absorption contrast for *in vivo*. Hence, NIR contrast may be best provided from the collection of NIR fluorescent photons rather than from the attenuation of excitation photons, which may occur from endogenous chromophores as well as from the exogenous fluorophores.

Herein, we present our work on a dual-labeled conjugate — (¹¹¹In-DTPA)_n-trastuzumab-(IRDye800)_m — which targets the human epidermal growth factor receptor-2 (HER2). Overexpression of HER2 is associated with poor prognosis in about 20 to 30% of breast cancer patients.¹⁷ We have previously shown specificity *in vivo* in subcutaneous xenograft models.¹⁸ In this report, we first review recent results from our group describing lymphatic imaging with nonspecific optical agents. Next, we review our prior results showing tumor targeting of dual-labeled (¹¹¹In-DTPA)_n-trastuzumab-(IRDye800)_m and enhanced performance of optical over nuclear imaging. We additionally show trafficking of the labeled antibody into the lymphatics and its subsequent drainage into lymph nodes using NIR optical imaging.

2 Real-Time Lymphatic Imaging with Near-Infrared Fluorophores

Recently, Sharma et al. illustrated the ability to quantitatively image lymph function in a swine model after administering an i.d. injection of a nonspecific NIR fluorophore, IC-Green.¹⁹ Their work was the first to noninvasively image pulsatile lymph flow velocities of 0.23 to 0.75 cm/s, averaging approximately 3.3 pulses/min along lymph channels ranging 2 to 16 cm in length. A similar approach was employed by Sevick-Muraca et al., who used i.d. microdoses (10 to 100 μg) of IC-Green to image lymph propulsion in the breast and axilla of breast cancer patients undergoing sentinel lymph node mapping.²⁰ They observed mean velocities ranging between 0.08 and 0.32 cm/s. The image acquisition time for optical imaging in both swine and humans ranged from 200 to 800 ms. Upon further reducing the integration time to 100 ms, Kwon and Sevick-Muraca have been able to rapidly image lymph trafficking in the limbs and tail of mice.²¹ The average lymph flow velocity ranged from 0.28 to 1.35 mm/s.

Figure 1 depicts representative optical images showing “packets” of IC-Green solution traversing the lymphatic channels after i.d. administration in human (b), swine (c), and mouse (d).^{19–21} The stick-diagram with a white light image (a) illustrates the right breast view of a breast cancer patient with four covered i.d. injection sites. The corresponding optical image from this patient (b) reveals two lymph channels and a region of lymph “pooling” through which IC-packets were propelled into the axilla. The swine model shows lymph propulsion from the hind limb up to the middle iliac node, while the mouse model depicts IC-Green trafficking to the axillary lymph node after i.d. administration into the footpad of the forepaw. These studies demonstrate the feasibility of noninvasive NIR optical imaging to qualitatively and quantitatively contribute toward the standard of care in nodal staging in preclinical and clinical studies. Most importantly, the human

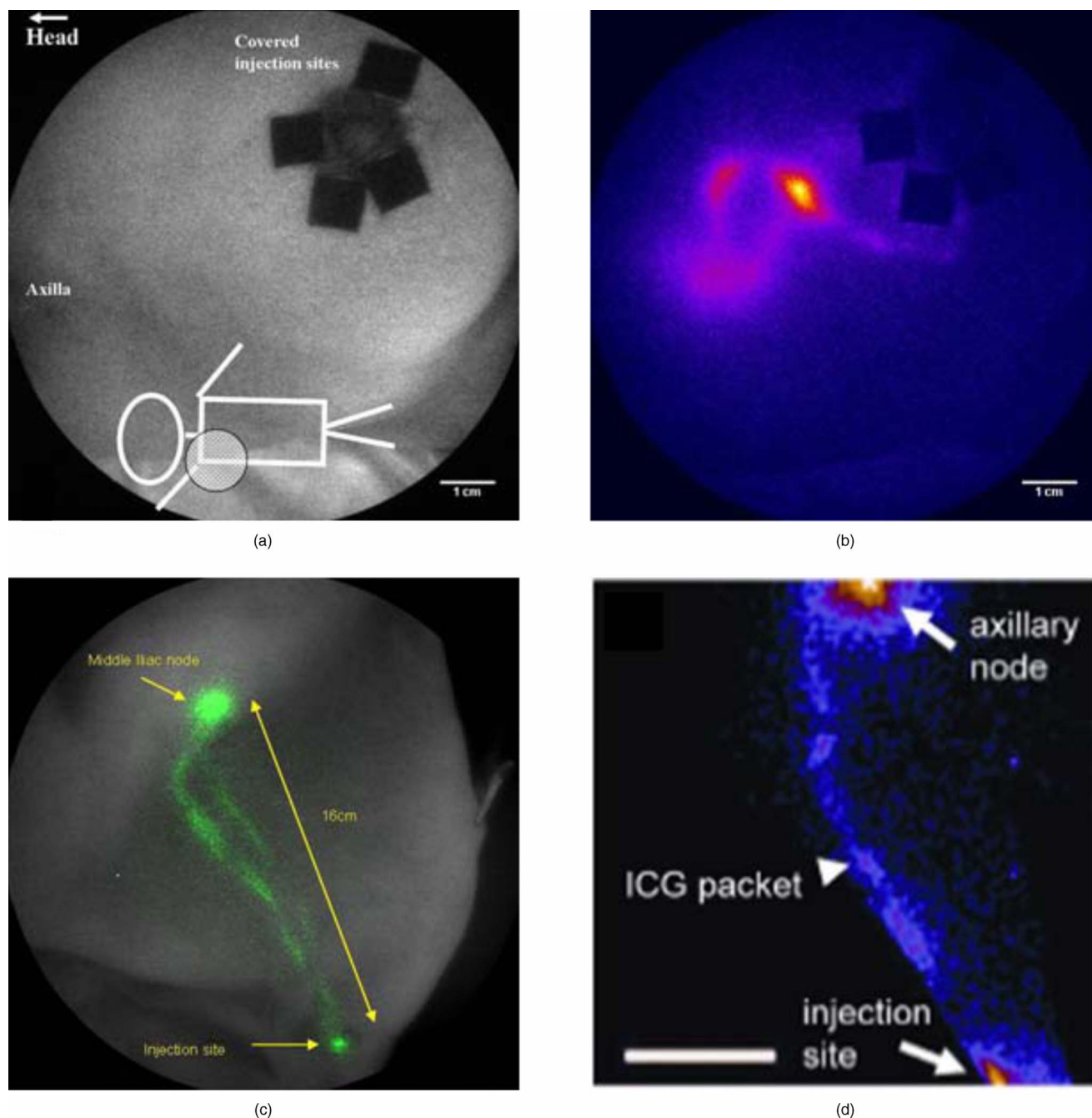


Fig. 1 (a) shows the white light image of a right breast from a patient who has been injected with IC-Green ($100 \mu\text{g}$) around the areola region. The injection sites have been covered to prevent oversaturation of the camera. (b) is the corresponding optical image, showing trafficking into the axillary lymph node. (c) is an overlay of optical imaging over the white light image of a swine's hind limb, showing IC-Green ($32 \mu\text{M}$) transiting to the middle iliac node after i.d. delivery. (d) shows the lymph trafficking of IC-Green (1.3 mM) to the axillary node of a mouse after i.d. injection into the footpad. All images have been reproduced with permission from Refs. 19–21.

studies confirm the ability to use microdose administration (i.e., between 10 and 100 micrograms) of IC-Green, suggesting that the instrumentation is capable of assessing NIR fluorescent signals for molecular imaging after trace administration of molecular imaging conjugate.

Other investigators have also conducted NIR fluorescence imaging of IC-Green. Frangioni and coworkers have intraoperatively imaged the fluorescence from IC-Green and other NIR fluorescent conjugates administered intradermally to in-

traoperatively identify sentinel lymph nodes in animal models.^{22–24} Yodh and coworkers²⁵ also measured fluorescence in humans after intravenous administration of 0.125 mg/kg . In their work, as well as in the work of others described earlier, NIR fluorescence was measured using an integrating CCD camera but was coupled with time-resolved absorbance measurements made in the frequency domain in order to perform fluorescence optical tomography from the

fluorescence CW measurements. To date, there have been no reports of fluorescence enhanced optical tomography using PMT-based, time-dependent measurements of fluorescence as reported in the companion review paper by Sevick-Muraca and Rasmussen.²⁶ Fluorescence tomography using gain modulation of an intensified CCD camera has been demonstrated in phantoms by Godavarty et al.,^{27,28} Roy et al.,²⁹ and Joshi et al.,³⁰ however, using mM amounts of IC-Green. Before fluorescence tomography measurements can be conducted using microdoses in clinically relevant tissue volumes, two requirements must be met: the “noise floor” of fluorescence measurements must be reduced,²⁶ and a molecularly targeting NIR optical imaging agent specific to disease must be used. Herein, we review and present new work on a dual-labeled imaging agent for planar NIR fluorescence imaging validated with nuclear imaging techniques.

3 Dual-Labeled Molecular Imaging Agents

Imaging agents that are designed with both nuclear and optical tracers combine complementary advantages from each modality and enhance the potential for detection of disease. Dual-labeled agents provide us with a unique opportunity to cross-validate NIR and nuclear imaging modalities. Some peptide-based dual-labeled imaging agents developed include a cyclopentapeptide, c(KRGDf), which is known to target alpha(v)beta3 integrins,^{31,32} and a cyclic peptide, c(CGRRAGGSC), which is known to target IL-11 Ref. 33. Quantitative comparison between planar scintigraphy and optical imaging in *in vivo* xenograft models injected with the RGD peptide have revealed comparable sensitivities between the two modalities, but NIR fluorescence shows improved signal-to-noise ratios.³² Herein, we employ the dual-labeling strategy to image antibodies in the lymphatics.

3.1 Labeled Trastuzumab for Metastasis and Nodal Staging

The human epidermal growth factor receptor (HER) family consists of transmembrane receptor tyrosine kinases that regulate complex intracellular signaling networks to control normal and pathological cellular growth, differentiation, and survival.³⁴ The second member, HER2, is of particular importance in breast cancer because overexpression or gene amplification of HER2 is closely associated with aggressive tumor progression and poor prognosis. Since a significant percentage of breast cancer patients are affected by the aberrant HER2 signaling, this family of receptors represents an excellent target for therapeutics. Additionally, the presence of HER2 on the plasma membrane of cells has also made it a potential target for diagnostic biomarkers. Trastuzumab (Herceptin, Genentech, San Francisco) is a humanized anti-HER2 antibody³⁵ that interferes with HER2 signaling and is approved clinically as a therapeutic for breast cancer.^{36,37} Evidence also suggests that with metastasis, HER2 is conserved or elevated with respect to that expressed on the primary tumors.^{38,39}

Several investigators have labeled intact, derived, and fragments [(Fab, F(ab')₂)] of trastuzumab antibody with a number of radioactive nuclear agents such as Ga-68 (Ref. 40), Y-90 (Refs. 41–43), In-111 (Refs. 41–43), and Tc-99m (Ref. 44) to image HER2 overexpressing breast cancer xenografts, as shown in Table 1. Smith-Jones et al.⁴⁰ showed

that sequential positron emission tomography (PET) imaging using ⁶⁸Ga-labeled F(ab')₂ fragments of trastuzumab can be used to quantify the loss and recovery of HER2 induced by HSP90 inhibitors in animals bearing BT-474 human breast tumors, while Tang et al.^{43,44} have developed In-111 and Tc-99m based trastuzumab Fab conjugates to detect xenografts using whole-body scintigraphy. Huh et al.⁴⁶ and Artemov et al.⁴⁷ have conjugated nanocrystals and iron-oxide-based nanoparticles to detect HER2 expression with magnetic resonance imaging (MRI). Optical imaging-based strategies include intact trastuzumab labeled with a red fluorescent dye to image HER2-overexpressing human breast cancer xenografts, as shown by Hilger et al.,⁴⁹ while recently Koyama et al. applied spectral fluorescence imaging methods with rhodamine-green conjugated trastuzumab to visualize pulmonary metastases.⁵⁰ Tada et al. have used a confocal scanner unit coupled with an EMCCD camera to track single quantum dot particles, which have been conjugated to trastuzumab, from a capillary vessel to a cancer cell in a live animal.⁵¹

The first use of trastuzumab as a diagnostic imaging agent was reported by Behr et al.⁵³ This was followed by a study by Perik et al. in which In-111-labeled trastuzumab was clinically translated for scintigraphy and systemic administration in patients (*n*=17) to help identify late-stage metastases with SPECT/CT imaging that was not previously identified.⁵⁴

3.2 Dual-Labeled Trastuzumab for Cancer Imaging

Recently, we have synthesized a dual-labeled antibody — (¹¹¹In-DTPA)_{*n*}-trastuzumab-(IRDye800)_{*m*} — and demonstrated imaging specificity for HER2 *in vitro* and *in vivo*. The reader is referred to Ref. 18 for details of synthesis and imaging. Figure 2 represents a schematic of the imaging agent. Since DTPA dianhydride and the NIR dye, IRDye 800CW, bind at the lysine residues of the antibody, we see a range in the ratios of binding between each of these molecules with trastuzumab, with *m* and *n* typically ranging between 7 and 10. The agent is stable at 4 °C for extended periods of time, but DTPA dianhydride shows serum-based instability with degradation occurring at the rate of 6% per day. As an alternative, we have since employed more stable forms of DTPA, such as p-SCN-Bz-DTPA, for chelation of In-111, a gamma emitter with a half life of 2.8 days.

The binding of (DTPA)_{*n*}-trastuzumab-(IRDye800)_{*m*} to a single SKBR3 cell that overexpresses HER2 is shown in Fig. 3. Sytox green stains the nucleus, while the fluorescent signal from IRDye 800CW indicating local expression of HER2 is present only along the outer rim of the cell, demonstrating extracellular binding. In Fig. 3 the nuclear stain is pseudo-colored green and (DTPA)_{*n*}-trastuzumab-(IRDye800)_{*m*} binding is represented in red. Prior incubation with unlabeled trastuzumab obliterates (DTPA)_{*n*}-trastuzumab-(IRDye800)_{*m*} cell binding, indicating the molecular specificity of the agent.¹⁸ Figure 3 also illustrates the usefulness of optical labeling in molecular imaging, as *in vitro* specificity can be readily visualized from microscopy, an advantage not present in nuclear imaging techniques.

Both nuclear and planar NIR fluorescence imaging was used to evaluate the *in vivo* specificity of (¹¹¹In-DTPA)_{*n*}-trastuzumab-(IRDye800)_{*m*}. Figure 4 shows a

Table 1 Summary of molecular imaging studies using trastuzumab.

Imaging Modality	Imaging Agent	<i>In vitro/In vivo:</i> Cell Lines Used	Dose	Route	Ref.
Nuclear medicine					
Position emission tomography (PET)	⁶⁴ Cu-DOTA-Herceptin ⁶⁸ Ga-DOTA-F(ab ²) ₂	<i>In vivo</i> (mice): BT-474 MCF-7, MDA-MB-468 (s.c.)	4 MBq 309 MBq	i.v.	40
Single photon emission computed tomography/computed tomography (SPECT/CT)	¹¹¹ In-DOTA-Fab4D5, ¹¹¹ In-DOTA-AB.Fab4D5	<i>In vivo</i> (mice): tumor cells derived from MMTV/HER2 transgenic mice (s.c.)	4 mg/kg (300 to 500 μ Ci)	i.v.	42
Scintigraphy (whole body)	[^{99m} Tc]-HYNIC-Trastuzumab Fab, ¹¹¹ In-trastuzumab Fab, ¹¹¹ In-DTPA-trastuzumab,	<i>In vivo</i> (mice): BT/474, SK-OV-3 (s.c.) <i>In vivo</i> (mice, humans)	25 MBq (30 μ g) 3.7 MBq (30 μ g) Mice: 450 \pm 25 kBq (25 μ g); Human: 100 to 150 MBq (5 mg)	i.v. i.v.	43 and 44, 45
Scintillation counter (tissue/cells)	¹¹¹ In-DOTA-Herceptin, ¹¹¹ In-DOTA-F(ab') ₂ , ¹¹¹ In-CHX-A''-DTPA-Herceptin, ⁹⁰ Y-DTPA-Herceptin	<i>In vivo</i> (mice): BT474 (s.c.) <i>In vitro</i> : MCF-7, SKBr-3	1.6 MBq 1 μ Ci/ml	i.v.	40 41
Magnetic resonance tomography (MRT)	WSIO-Herceptin Biotinylated Herceptin with Streptavidin-SPIO microbeads	<i>In vitro</i> NIC3T6.7 (s.c.) <i>In vitro</i> : MCF-7, MDA-MB-231, AU-565 (gel phantoms)	400 μ g of Fe 2 to 50 10 ¹⁰ biotin/ μ l	i.v.	46 and 47
Optoacoustic tomography (OT)	Herceptin conjugated with gold nanoparticles (MabNP)	<i>In vivo</i> : SK-BR-3, L6 rat myoblasts	10 ⁹ Mab/NP		48
Optical imaging					
Fluorescence imaging	Cy5.5-labeled Herceptin Herceptin-RhodG	<i>In vivo</i> (mice): SK-BR-3, PE/CA-PJ34 (s.c.) <i>In vivo</i> (mice): 3T3/HER2+, Balb/3T3/HER2-	100 μ g 50 μ g in 200 μ l PBS	i.v. i.v.	49 50
Fluorescence quantum dots	Trastuzumab-Qdots	<i>In vivo</i> (mice), <i>ex vivo</i> (tumor from mice): KPL-4, MBA-MB-231 (s.c.)	2 μ mol/L (100 μ l), 5–6 μ m tissue sections stained with 10 μ M	i.v.	51 and 52

series of whole-body fluorescence (a and b), planar scintigraphy (c), and SPECT/CT (d) images from athymic nude mice with HER2-overexpressing SKBr3 human breast cancer xenografts after i.v. injection of (¹¹¹In-DTPA)_n-trastuzumab-(IRDye800)_m. *In vivo* fluorescence imaging was accomplished by illuminating the animal with light from a laser diode (85 mA and 80 mW for 785-nm light; DL7140-201; Sanyo) that expanded to a circular area approximately 8 cm in diameter. The reemitted fluorescent light was collected with an EMCCD camera in CW mode. Filter sets used in this study

included a bandpass filter with an 830-nm center wavelength and an optical density of greater than 3 at 785 nm (ANDV8483; Andover Corp.) for collecting IRDye 800CW fluorescence and a holographic filter with an optical density of greater than 6 (HSP 785.0; Kaiser Optical Systems) for rejecting backscattered and reflected excitation light. Image acquisition was accomplished with V11 software to collect raw fluorescence images, and with these images, data processing and analysis were accomplished with ImageJ software. The integration time for white-light and fluorescence images was

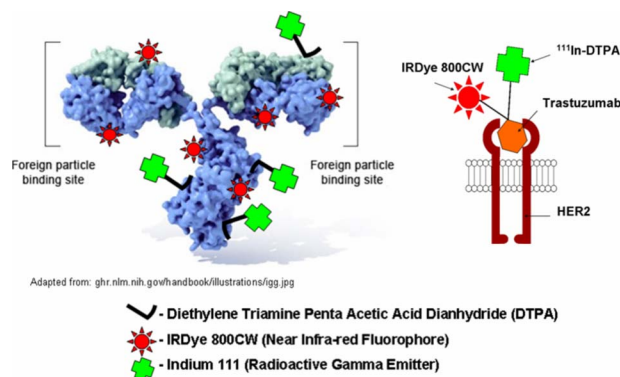


Fig. 2 Schematic of $(^{111}\text{In-DTPA})_n\text{-trastuzumab-(IRDye800)}_m$.

800 ms. SPECT and CT images were acquired consecutively with a MicroCAT II scanner (Siemens Medical Solutions). The SPECT scan was acquired for 20 projections over 360 day for a scan time of 1 min per frame. SPECT and CT tomographic images were coregistered by geometric transformation and rendered to make the fused images with Amira (version 3.1; Konrad-Zuse-Zentrum fur Informationstechnik). Planar scintigraphy was performed by removing the 3-mm pinhole collimator of the SPECT scanner, adding a 1.22-mm planar collimator, and integrating for 10 min.

The fluorescence and nuclear signal obtained at the tumor region appear significantly higher than the rest of the body. Comparison of tumor uptake between mice after administration of dye alone and dual-labeled trastuzumab revealed significant accumulation of the dual-labeled agent in the tumor, as opposed to dye alone (p -value: 0.0011). Antibody interaction with the hepatocytes (which represent routes for degradation and clearance) increased agent accumulation in the liver and is expected with i.v. administration of an antibody-based imaging agent. Liver uptake is observed in both imaging modalities, consistent with the integrity of the dual-labeled agent.

The target-to-muscle ratios (TMRs) calculated from the planar fluorescence and planar scintigraphy images according to the approach described by Houston et al.³² are found to be comparable at 2.11 and 2.43, respectively, and consistent with the dual labeling on a single imaging agent. The signal-to-

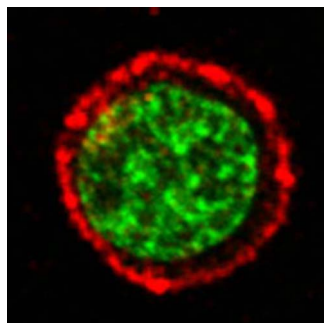


Fig. 3 Confocal image of one SKBr3 cell after incubation with $(\text{DTPA})_n\text{-trastuzumab-(IRDye800)}_m$. Nuclear staining is by sytox green and is pseudo-colored in green, while fluorescence from IRDye 800 is represented in red. (Color online only.)

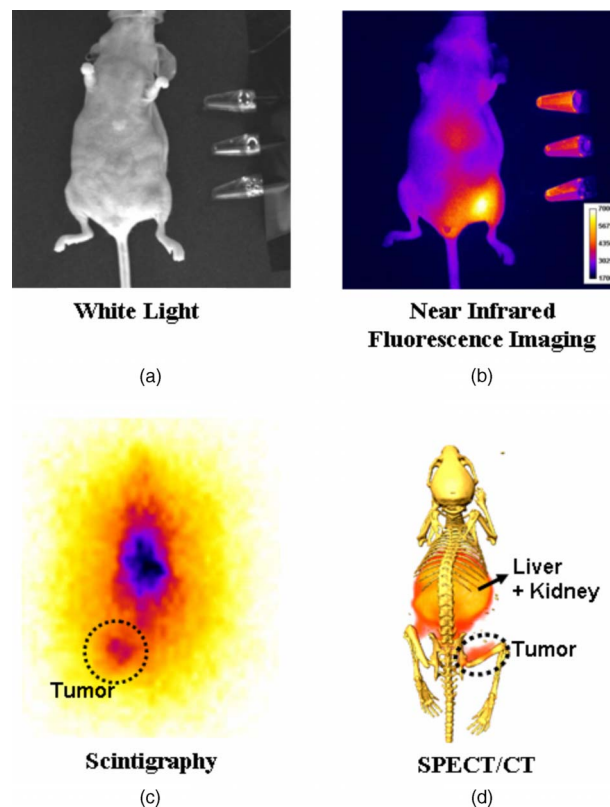


Fig. 4 (a) and (b) are representative white light and whole-body fluorescence images of an athymic nude mouse inoculated with SKBr3-luc xenografts, taken 48 h after i.v. administration of $(^{111}\text{In-DTPA})_n\text{-trastuzumab-(IRDye800)}_m$. High agent uptake is visible in the left flank, which is consistent with the tumor region. Similar uptake is observed in nuclear imaging obtained from ^{111}In , as represented by planar scintigraphy (c) and SPECT/CT (d). Reproduced from Ref. 18.

noises ratio (SNRs) calculated from the planar fluorescence and planar scintigraphy images are found to be dramatically different at 16.82 and 4.22, respectively. The differences can be attributed to the increased photon count rates of fluorescence imaging when compared to scintigraphy. Upon dissection of major organs and evaluation of gamma and fluorescent photon counts, the TMRs were calculated for both modalities. When optical TMR is normalized by area (or pixels) and nuclear TMR by tissue weight (in grams), no significant change is observed within each modality over time, but the signal obtained from optical imaging is statistically higher compared to that from nuclear imaging. In contrast, when both TMRs are calculated based on tissue weight, the statistical significance disappears, as represented by Fig. 5, consistent with the origin of both nuclear and fluorescent signals from a single imaging agent. In addition, the standard error observed in optical imaging is smaller than nuclear imaging, consistent with the reduced SNR also observed in the case of the cyclic RGD peptide.³²

Further, we assessed the potential of antibody-based optical imaging for lymph node imaging using i.d. administration. Upon injecting $1\ \mu\text{g}$ (5.4 pmole) of a $1\ \mu\text{g}/\mu\text{l}$ solution into the footpad of athymic nude mice, we were able to image trafficking of $(\text{In-DTPA})_n\text{-trastuzumab-(IRDye800)}_m$ into

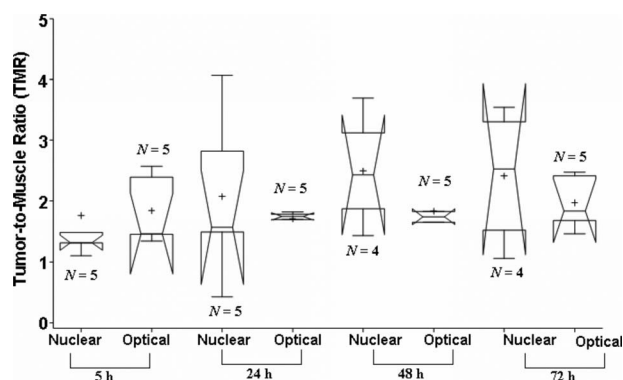


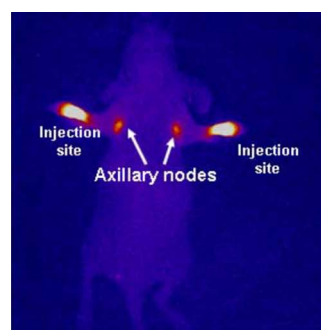
Fig. 5 Plot of nuclear versus optical tumor-to-muscle ratios (TMRs), normalized per gram of tissue. No statistical differences have been observed, but optical imaging with smaller error bars indicates higher signal-to-noise ratios (SNRs). Reproduced from Ref. 18.

the axillary nodes and popliteal nodes [Figs. 6(a) and 6(b), respectively]. A closer look at the popliteal lymph nodes, revealed lymphatic channels that picked up the agent from the injection site and drained it into the lymph node as indicated by the arrows in Fig. 6(c). Both images were obtained within 1 h of injection. It is of interest to note that the volume injected in our preclinical study is considerably less when compared to the 50 to 200 μl injections as reported with nuclear imaging.^{2,3}

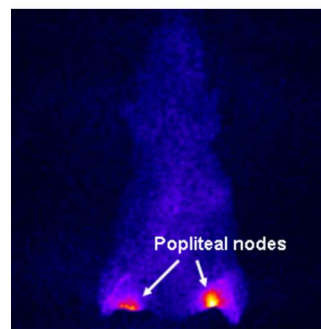
Figure 7(b) shows a sequence of optical images taken after an i.d. injection of $(\text{In-DTPA})_n\text{-trastuzumab-(IRDye800)}_m$ (1 μg , 5.4 pmole) into the footpad of an athymic mouse. The lymph node targeted was the axillary node. The corresponding sample white light image is shown in Fig. 7(a). The accumulation and clearance of the antibody-based imaging agent in the lymph node is slower than that observed by IC-Green or IRDye 800CW. IRDye 800CW has a molecular weight of 1166 Da, which is significantly smaller than antibodies (MW: 185kDa), enabling it to clear from the lymph nodes within a few hours. Antibodies requires a few days (data not shown), which can be a problem for radioimmunosciintigraphy of cancer-positive lymph nodes. Figure 7(c) shows the rate of clearance of $(\text{In-DTPA})_n\text{-trastuzumab-(IRDye800)}_m$ averaged over time in five animals. We found variability in the uptake of the imaging agent into the axillary node among the mice, which is represented by a large error bar at $t=0$ h [Fig. 7(c)], but all mice attained maximum fluorescence in nodes within $t=1$ h. The half-life of clearance was between 10 to 12 h, which is consistent with previous reports using radio-labeled antibodies. As seen in the i.v. administration of $(\text{In-DTPA})_n\text{-trastuzumab-(IRDye800)}_m$, we also observed a fluorescence signal emanating from the liver region after an i.d. injection (albeit at later times), which is consistent with antibody degradation and clearance.

4 Conclusion

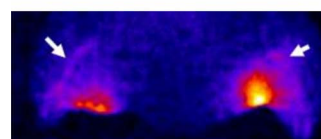
This study demonstrates the potential of using NIR fluorescence imaging for impacting tumor nodal staging. By enhancing the accuracy of nodal staging with molecular-specific imaging agents, we can offer novel approaches to diagnose sites that are often harder to access for *ex vivo* pathology, e.g.,



(a)



(b)



(c)

Fig. 6 Intradermal injection trastuzumab-(IRDye800)_m in the footpads of mice show trafficking to the axillary nodes (a) and popliteal nodes (b). The injection site has been covered in (b). A higher magnification of the region around the popliteal nodes shows lymphatic channels that drain into the node (c).

internal mammary nodes and supraclavicular nodes in breast and pelvic lymph nodes in prostate cancer patients. By injecting the agent directly into lymphatics through i.d. or s.c. routes, we can considerably reduce the dose administered and the amount of nonspecific binding in other organs that is characteristic of an i.v. route of administration. Since antibodies are cleared through the liver and kidneys, which are major organs surrounding the lymph nodes draining the prostate, i.d. delivery is especially advantageous in assessing metastases in prostate cancer.

Despite nuclear imaging being the clinical “gold standard” of molecular imaging, optical imaging provides superior signal-to-noise ratios with low camera integration times due to high photon count rate. These advantages have recently provided investigators with an opportunity to analyze lymph function and quantify pulsatility in humans, swine, and mice.^{19–21} Furthermore, they have enabled the synthesis of novel optical-based targeting agents to address other lymph-based disorders, as demonstrated by HA-NIR, a molecular target of the lymph vascular endothelial receptor (LYVE-1).¹⁹ In the present study, we have shown the feasibility of performing optical imaging in detecting lymph nodes in a pre-

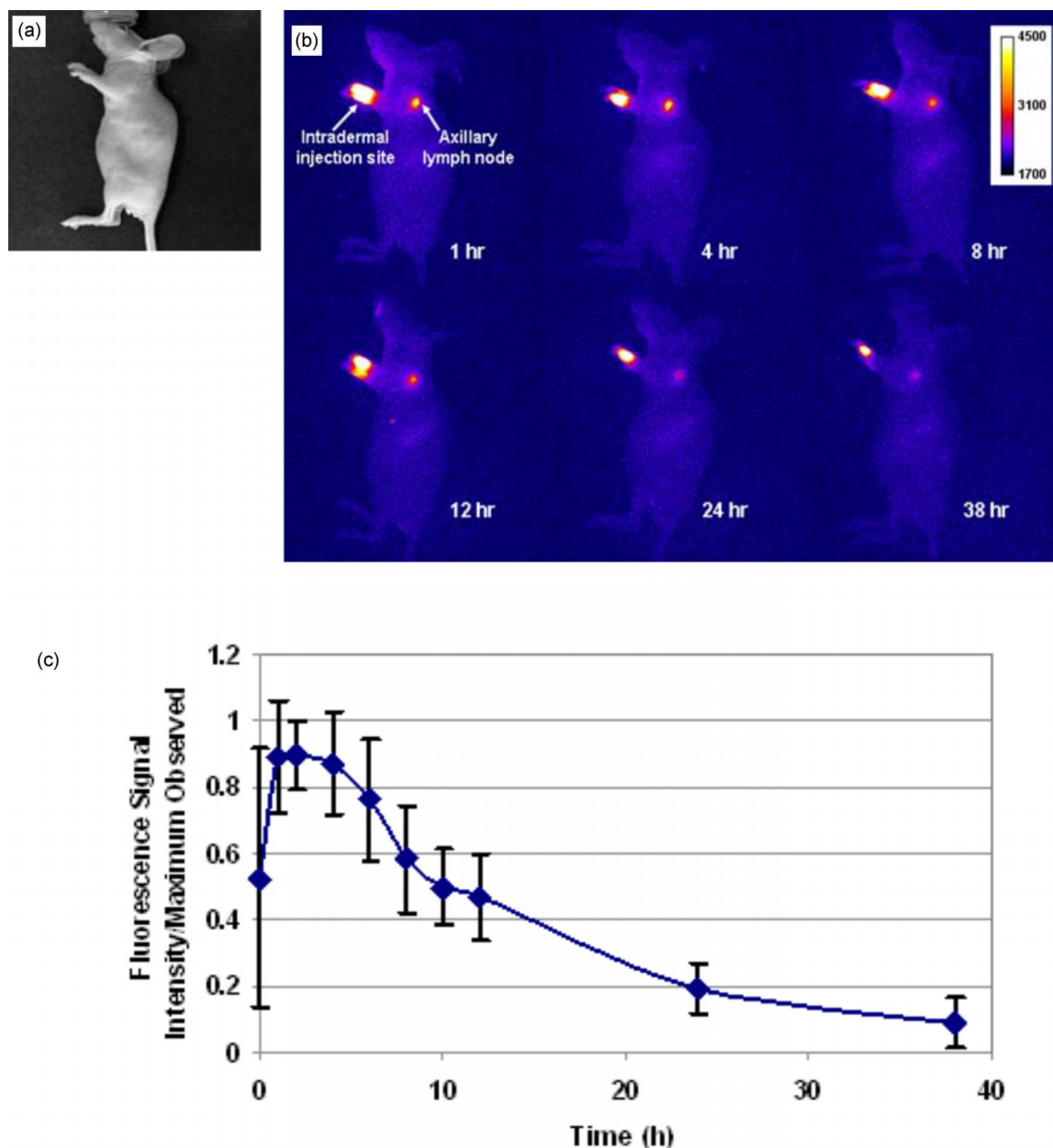


Fig. 7 Representative white light (a) and optical imaging (b) of accumulation and clearance of $(\text{In-DTPA})_n\text{-trastuzumab-(IRDye800)}_m$ ($1 \mu\text{g}$, 5.4 pmole) in the axillary node after administration into the forepaw footpad. Quantitative analysis of lymph node trafficking in five mice is represented in (c).

clinical animal model using molecular targets such as antibodies. $(^{111}\text{In-DTPA})_n\text{-trastuzumab-(IRDye800)}_m$ is a dual-labeled antibody that exhibits high molecular specificity to HER2. We have demonstrated that picomole amounts are sufficient to visualize the axillary and popliteal lymph nodes in mice (Fig. 6). We observed that the fluorescent intensity due to dual-labeled $(\text{In-DTPA})_n\text{-trastuzumab-(IRDye800)}_m$ reduced to half of its highest value at 12 h after administration [Fig. 7(c)]. But further studies addressing questions of specificity and sensitivity will have to be conducted to prove efficacy for cancer detection. Nonetheless, the combination of NIR and nuclear imaging of lymph node metastases in cancer patients with dual-labeled molecular agents that are adminis-

tered through i.d. or s.c. routes shows promise for improving the accuracy of tumor node metastasis staging.

Acknowledgments

This work was supported by the National Institutes of Health, Grant Nos. P50 CA58183, R01 EB003132, and R01 CA112679.

References

1. J. N. Weinstein, R. J. Parker, A. M. Keenan, S. K. Dower, H. C. Morse III, and S. M. Sieber, "Monoclonal antibodies in the lymphatics: toward the diagnosis and therapy of tumor metastases," *Science* **218**(4579), 1334–1337 (1982).

2. J. N. Weinstein, M. A. Steller, A. M. Keenan, D. G. Covell, M. E. Key, S. M. Sieber, R. K. Oldham, K. M. Hwang, and R. J. Parker, "Monoclonal antibodies in the lymphatics: selective delivery to lymph node metastases of a solid tumor," *Science* **222**(4622), 423–426 (1983).
3. M. A. Steller, R. J. Parker, D. G. Covell, O. D. Holton III, A. M. Keenan, S. M. Sieber, and J. N. Weinstein, "Optimization of monoclonal antibody delivery via the lymphatics: the dose dependence," *Cancer Res.* **46**(4 Pt. 1), 1830–1834 (1986).
4. R. L. Wahl, O. Geatti, M. Liebert, B. Wilson, P. Shreve, and B. A. Beers, "Kinetics of interstitially administered monoclonal antibodies for purposes of lymphoscintigraphy," *J. Nucl. Med.* **28**(11), 1736–1744 (1987).
5. J. L. Mulshine, A. M. Keenan, J. A. Carrasquillo, T. Walsh, R. I. Linnoila, O. D. Holton, J. Harwell, S. M. Larson, P. A. Bunn, and J. N. Weinstein, "Immunolymphoscintigraphy of pulmonary and mediastinal lymph nodes in dogs: a new approach to lung cancer imaging," *Cancer Res.* **47**(13), 3572–3576 (1987).
6. C. J. Porter and S. A. Charman, "Lymphatic transport of proteins after subcutaneous administration," *J. Pharm. Sci.* **89**(3), 297–310 (2000).
7. S. E. Order, W. D. Bloomer, A. G. Jones, W. D. Kaplan, M. A. Davis, S. J. Adelstein, and S. Hellman, "Radionuclide immunoglobulin lymphangiography: a case report," *Cancer* **35**(6), 1487–1492 (1975).
8. F. H. DeLand, E. E. Kim, and D. M. Goldenberg, "Lymphoscintigraphy with radionuclide-labeled antibodies to carcinoembryonic antigen," *Cancer Res.* **40**(8 Pt. 2), 2997–3000 (1980).
9. J. J. Tjandra, I. S. Russell, J. P. Collins, J. T. Andrews, M. Lichtenstein, D. Binns, and I. F. McKenzie, "Immunolymphoscintigraphy for the detection of lymph node metastases from breast cancer," *Cancer Res.* **49**(6), 1600–1608 (1989).
10. K. J. Kairemo, "Immunolymphoscintigraphy with ^{99m}Tc-labeled monoclonal antibody (BW 431/26) reacting with carcinoembryonic antigen in breast cancer," *Cancer Res.* **50**(3 Suppl.), 949s–954s (1990).
11. A. M. Keenan, J. N. Weinstein, J. L. Mulshine, J. A. Carrasquillo, P. A. Bunn Jr., J. C. Reynolds, and S. M. Larson, "Immunolymphoscintigraphy in patients with lymphoma after subcutaneous injection of indium-111-labeled T101 monoclonal antibody," *J. Nucl. Med.* **28**(1), 42–46 (1987).
12. A. M. Keenan, J. N. Weinstein, J. A. Carrasquillo, P. A. Bunn Jr., J. C. Reynolds, K. A. Foon, N. C. Smarte, B. Ghosh, R. M. Fejka, S. M. Larson, et al., "Immunolymphoscintigraphy and the dose dependence of ¹¹¹In-labeled T101 monoclonal antibody in patients with cutaneous T-cell lymphoma," *Cancer Res.* **47**(22), 6093–6099 (1987).
13. H. H. Abdel-Nabi, J. A. Ortman-Nabi, W. See, J. Lee, R. Ireton, M. Boileau, M. W. Unger, and C. Halverson, "Clinical experience with intralymphatic administration of ¹¹¹In-labeled monoclonal antibody PAY 276 for the detection of pelvic nodal metastases in prostatic carcinoma," *Eur. J. Nucl. Med.* **16**(3), 149–156 (1990).
14. M. T. Lotze, J. A. Carrasquillo, J. N. Weinstein, G. J. Bryant, P. Perentesis, J. C. Reynolds, L. A. Matis, R. R. Eger, A. M. Keenan, I. Hellstrom, et al., "Monoclonal antibody imaging of human melanoma. Radioimmuno-detection by subcutaneous or systemic injection," *Ann. Surg.* **204**(3), 223–235 (1986).
15. W. B. Nelp, J. F. Eary, R. F. Jones, K. E. Hellstrom, I. Hellstrom, P. L. Beaumier, and K. A. Krohn, "Preliminary studies of monoclonal antibody lymphoscintigraphy in malignant melanoma," *J. Nucl. Med.* **28**(1), 34–41 (1987).
16. B. L. Engelstad, L. E. Spittler, M. J. Del Rio, E. C. Ramos, L. L. Rosendorf, C. E. Reinhold, A. Khentigan, J. P. Huberty, S. W. Corpuz, H. M. Lee, et al., "Phase I immunolymphoscintigraphy with an In-111-labeled antimelanoma monoclonal antibody," *Radiology* **161**(2), 419–422 (1986).
17. D. J. Slamon, W. Godolphin, L. A. Jones, J. A. Holt, S. G. Wong, D. E. Keith, W. J. Levin, S. G. Stuart, J. Udove, A. Ullrich, et al., "Studies of the HER-2/neu proto-oncogene in human breast and ovarian cancer," *Science* **244**(4905), 707–712 (1989).
18. L. Sampath, S. Kwon, S. Ke, W. Wang, R. Schiff, M. E. Mawad, and E. M. Sevick, "Dual-labeled trastuzumab-based imaging agent for the detection of human epidermal growth factor receptor-2 (HER2) overexpression in breast cancer," *J. Nucl. Med.* **48**(9), 1501–1510 (2007).
19. R. Sharma, W. Wang, J. C. Rasmussen, A. Joshi, J. P. Houston, K. E. Adams, A. G. Cameron, S. Ke, S. Kwon, M. E. Mawad, and E. M. Sevick, "Quantitative imaging of lymph function," *Am. J. Physiol. Heart Circ. Physiol.* **292**, H3109–H3118 (2007).
20. E. M. Sevick-Muraca, R. Sharma, J. C. Rasmussen, M. V. Marshall, J. A. Wendt, H. Q. Pham, E. Bonefas, J. P. Houston, L. Sampath, K. E. Adams, D. K. Blanchard, R. E. Fisher, S. B. Chiang, R. Elledge, and M. E. Mawad, "Imaging of lymph flow in breast cancer patients after microdose administration of a near-infrared fluorophore: feasibility study," *Radiology* **246**(3), 734–741 (2008).
21. S. Kwon and E. M. Sevick-Muraca, "Noninvasive quantitative imaging of lymph function in mice," *Lymphatic Res. Biol.* **5**(4), 219–231 (2007).
22. D. W. Knapp, L. G. Adams, A. M. Degrand, J. D. Niles, J. A. Ramos-Vara, A. B. Weil, M. A. O'Donnell, M. D. Lucroy, and J. V. Frangioni, "Sentinel lymph node mapping of invasive urinary bladder cancer in animal models using invisible light," *Eur. Urol.* **52**(6), 1700–1708 (2007).
23. C. P. Parungo, D. I. Soybel, Y. L. Colson, S. W. Kim, S. Ohnishi, A. M. DeGrand, R. G. Laurence, E. G. Soltesz, F. Y. Chen, L. H. Cohn, M. G. Bawendi, and J. V. Frangioni, "Lymphatic drainage of the peritoneal space: a pattern dependent on bowel lymphatics," *Ann. Surg. Oncol.* **14**(2), 286–298 (2007).
24. E. Tanaka, S. Ohnishi, R. G. Laurence, H. S. Choi, V. Humblet, and J. V. Frangioni, "Real-time intraoperative ureteral guidance using invisible near-infrared fluorescence," *J. Urol. (Baltimore)* **178**(5), 2197–2202 (2007).
25. A. Corlu, R. Choe, T. Durduran, M. A. Rosen, M. Schweiger, S. R. Arridge, and A. G. Yodh, "Three-dimensional *in vivo* fluorescence diffuse optical tomography of breast cancer in humans," *Opt. Express* **15**(11), 6696–6716 (2007).
26. E. M. Sevick-Muraca and J. C. Rasmussen, "Molecular imaging with optics: a primer and a case for near-infrared fluorescence techniques in personalized medicine," *J. Biomed. Opt.* **13**(4), 041305 (2008).
27. A. Godavarty, M. J. Eppstein, C. Zhang, and E. M. Sevick-Muraca, "Detection of single and multiple targets in tissue phantoms with fluorescence-enhanced optical imaging: feasibility study," *Radiology* **235**(1), 148–154 (2005).
28. A. Godavarty, C. Zhang, M. J. Eppstein, and E. M. Sevick-Muraca, "Fluorescence-enhanced optical imaging of large phantoms using single and simultaneous dual point illumination geometries," *Med. Phys.* **31**(2), 183–190 (2004).
29. R. Roy, A. Godavarty, and E. M. Sevick-Muraca, "Fluorescence-enhanced optical tomography of a large tissue phantom using point illumination geometries," *J. Biomed. Opt.* **11**(4), 044007 (2006).
30. A. Joshi, W. Bangerth, K. Hwang, J. C. Rasmussen, and E. M. Sevick-Muraca, "Fully adaptive FEM based fluorescence optical tomography from time-dependent measurements with area illumination and detection," *Med. Phys.* **33**(5), 1299–1310 (2006).
31. C. Li, W. Wang, Q. Wu, S. Ke, J. Houston, E. Sevick-Muraca, L. Dong, D. Chow, C. Charnsangavej, and J. G. Gelovani, "Dual optical and nuclear imaging in human melanoma xenografts using a single targeted imaging probe," *Nucl. Med. Biol.* **33**(3), 349–358 (2006).
32. J. P. Houston, S. Ke, W. Wang, C. Li, and E. M. Sevick-Muraca, "Quality analysis of *in vivo* near-infrared fluorescence and conventional gamma images acquired using a dual-labeled tumor-targeting probe," *J. Biomed. Opt.* **10**(5), 054010 (2005).
33. W. Wang, S. Ke, S. Kwon, S. Yallampalli, A. G. Cameron, K. E. Adams, M. E. Mawad, and E. M. Sevick-Muraca, "A new optical and nuclear dual-labeled imaging agent targeting interleukin 11 receptor alpha-chain," *Bioconjugate Chem.* **18**(2), 397–402 (2007).
34. Y. Yarden, "Biology of HER2 and its importance in breast cancer," *J. Surg. Oncol., Suppl.* **61**(Suppl 2), 1–13 (2001).
35. P. Carter, L. Presta, C. M. Gorman, J. B. Ridgway, D. Henner, W. L. Wong, A. M. Rowland, C. Kotts, M. E. Carver, and H. M. Shepard, "Humanization of an anti-p185HER2 antibody for human cancer therapy," *Proc. Natl. Acad. Sci. U.S.A.* **89**(10), 4285–4289 (1992).
36. E. Tokunaga, E. Oki, K. Nishida, T. Koga, A. Egashira, M. Morita, Y. Kakeji, and Y. Maehara, "Trastuzumab and breast cancer: developments and current status," *Int. J. Clin. Oncol.* **11**(3), 199–208 (2006).
37. C. H. Yeon and M. D. Pegram, "Anti-erbB-2 antibody trastuzumab in the treatment of HER2-amplified breast cancer," *Invest New Drugs* **23**(5), 391–409 (2005).
38. R. Simon, A. Nocito, T. Hubscher, C. Bucher, J. Torhorst, P. Schraml, L. Bubendorf, M. M. Mihatsch, H. Moch, K. Wilber, A. Schotzau, J. Kononen, and G. Sauter, "Patterns of HER-2/neu amplification and overexpression in primary and metastatic breast cancer," *J. Natl. Cancer Inst.* **93**(15), 1141–1146 (2001).

39. P. Regitnig, W. Schippinger, M. Lindbauer, H. Samonigg, and S. F. Lax, "Change of HER-2/neu status in a subset of distant metastases from breast carcinomas," *J. Pathol.* **203**(4), 918–926 (2004).
40. P. M. Smith-Jones, D. B. Solit, T. Akhurst, F. Afroze, N. Rosen, and S. M. Larson, "Imaging the pharmacodynamics of HER2 degradation in response to Hsp90 inhibitors," *Nat. Biotechnol.* **22**(6), 701–706 (2004).
41. M. J. Blend, J. J. Stastny, S. M. Swanson, and M. W. Brechbiel, "Labeling anti-HER2/neu monoclonal antibodies with ¹¹¹In and ⁹⁰Y using a bifunctional DTPA chelating agent," *Cancer Biother. Radiopharm.* **18**(3), 355–363 (2003).
42. M. S. Dennis, H. Jin, D. Dugger, R. Yang, L. McFarland, A. Ogasawara, S. Williams, M. J. Cole, S. Ross, and R. Schwall, "Imaging tumors with an albumin-binding Fab, a novel tumor-targeting agent," *Cancer Res.* **67**(1), 254–261 (2007).
43. Y. Tang, J. Wang, D. A. Scollard, H. Mondal, C. Holloway, H. J. Kahn, and R. M. Reilly, "Imaging of HER2/neu-positive BT-474 human breast cancer xenografts in athymic mice using (¹¹¹In)-trastuzumab (Herceptin) Fab fragments," *Nucl. Med. Biol.* **32**(1), 51–58 (2005).
44. Y. Tang, D. Scollard, P. Chen, J. Wang, C. Holloway, and R. M. Reilly, "Imaging of HER2/neu expression in BT-474 human breast cancer xenografts in athymic mice using [(^{99m}Tc)-HYNIC-trastuzumab (Herceptin) Fab fragments," *Nucl. Med. Commun.* **26**(5), 427–432 (2005).
45. M. N. Lub-de Hooge, J. G. Kosterink, P. J. Perik, H. Nijhuis, L. Tran, J. Bart, A. J. Suurmeijer, S. de Jong, P. L. Jager, and E. G. de Vries, "Preclinical characterisation of ¹¹¹In-DTPA-trastuzumab," *Br. J. Pharmacol.* **143**(1), 99–106 (2004).
46. Y. M. Huh, Y. W. Jun, H. T. Song, S. Kim, J. S. Choi, J. H. Lee, S. Yoon, K. S. Kim, J. S. Shin, J. S. Suh, and J. Cheon, "In vivo magnetic resonance detection of cancer by using multifunctional magnetic nanocrystals," *J. Am. Chem. Soc.* **127**(35), 12387–12391 (2005).
47. D. Artemov, N. Mori, B. Okollie, and Z. M. Bhujwala, "MR molecular imaging of the HER-2/neu receptor in breast cancer cells using targeted iron oxide nanoparticles," *Magn. Reson. Med.* **49**(3), 403–408 (2003).
48. J. A. Copland, M. Eghtedari, V. L. Popov, N. Kotov, N. Mamedova, M. Motamedi, and A. A. Oraevsky, "Bioconjugated gold nanoparticles as a molecular based contrast agent: implications for imaging of deep tumors using optoacoustic tomography," *Mol. Imaging Biol.* **6**(5), 341–349 (2004).
49. I. Hilger, Y. Leistner, A. Berndt, C. Fritsche, K. M. Haas, H. Kosmehl, and W. A. Kaiser, "Near-infrared fluorescence imaging of HER-2 protein over-expression in tumour cells," *Eur. Radiol.* **14**(6), 1124–1129 (2004).
50. Y. Koyama, Y. Hama, Y. Urano, D. M. Nguyen, P. L. Choyke, and H. Kobayashi, "Spectral fluorescence molecular imaging of lung metastases targeting HER2/neu," *Clin. Cancer Res.* **13**(10), 2936–2945 (2007).
51. H. Tada, H. Higuchi, T. M. Wanatabe, and N. Ohuchi, "In vivo real-time tracking of single quantum dots conjugated with monoclonal anti-HER2 antibody in tumors of mice," *Cancer Res.* **67**(3), 1138–1144 (2007).
52. S. Li-Shishido, T. M. Watanabe, H. Tada, H. Higuchi, and N. Ohuchi, "Reduction in nonfluorescence state of quantum dots on an immunofluorescence staining," *Biochem. Biophys. Res. Commun.* **351**(1), 7–13 (2006).
53. T. M. Behr, M. Behe, and B. Wormann, "Trastuzumab and breast cancer," *N. Engl. J. Med.* **345**(13), 995–996 (2001).
54. P. J. Perik, M. N. Lub-De Hooge, J. A. Gietema, W. T. van der Graaf, M. A. de Korte, S. Jonkman, J. G. Kosterink, D. J. van Veldhuisen, D. T. Sleijfer, P. L. Jager, and E. G. de Vries, "Indium-111-labeled trastuzumab scintigraphy in patients with human epidermal growth factor receptor 2-positive metastatic breast cancer," *J. Clin. Oncol.* **24**(15), 2276–2282 (2006).